EUROPEAN ORGANIZATION FOR NUCLEAR RESEARCH (CERN)

Search for R-Parity Violating Production of Single Sneutrinos in e$^+$e$^-$ Collisions at $\sqrt{s} = $ 189–209 GeV

The ALEPH Collaboration[*])

Abstract

A search for single sneutrino production under the assumption that R-parity is violated via a single dominant $LL\bar{E}$ coupling is presented. This search considers the process $e\gamma \to \tilde{\nu}\ell$ and is performed using the data collected by the ALEPH detector at centre-of-mass energies from 189 GeV up to 209 GeV corresponding to an integrated luminosity of 637.1 pb^{-1}. The numbers of observed candidate events are in agreement with Standard Model expectations and 95% confidence level upper limits on five of the $LL\bar{E}$ couplings are given as a function of the assumed sneutrino mass.

---

[*]) See next pages for the list of authors

The ALEPH Collaboration

A. Heister, S. Schael

Physikalisches Institut das RWTH-Aachen, D-52056 Aachen, Germany

R. Barate, R. Brunelière, I. De Bonis, D. Decamp, C. Goy, S. Jezequel, J.-P. Lees, F. Martin, E. Merle, M.-N. Minard, B. Pietrzyk, B. Trocmé

Laboratoire de Physique des Particules (LAPP), IN²P³-CNRS, F-74019 Annecy-le-Vieux Cedex, France

G. Boix, S. Bravo, M.P. Casado, M. Chmeissani, J.M. Crespo, E. Fernandez, M. Fernandez-Bosman, Ll. Garrido,[15] E. Graugés, J. Lopez, M. Martinez, G. Merino, R. Miquel,[31] Ll.M. Mir,[31] A. Pacheco, D. Paneque, H. Ruiz

Institut de Física d'Altes Energies, Universitat Autònoma de Barcelona, E-08193 Bellaterra (Barcelona), Spain[7]

A. Colaleo, D. Creanza, N. De Filippis, M. de Palma, G. Iaselli, G. Maggi, M. Maggi, S. Nuzzo, A. Ranieri, G. Raso,[24] F. Ruggieri, G. Selvaggi, L. Silvestris, P. Tempesta, A. Tricomi,[3] G. Zito

Dipartimento di Fisica, INFN Sezione di Bari, I-70126 Bari, Italy

X. Huang, J. Lin, Q. Ouyang, T. Wang, Y. Xie, R. Xu, S. Xue, J. Zhang, L. Zhang, W. Zhao

Institute of High Energy Physics, Academia Sinica, Beijing, The People's Republic of China[8]

D. Abbaneo, P. Azzurri, T. Barklow,[30] O. Buchmüller,[30] M. Cattaneo, F. Cerutti, B. Clerbaux, H. Drevermann, R.W. Forty, M. Frank, F. Gianotti, T.C. Greening,[26] J.B. Hansen, J. Harvey, D.E. Hutchcroft, P. Janot, B. Jost, M. Kado,[31] P. Maley, P. Mato, A. Moutoussi, F. Ranjard, L. Rolandi, D. Schlatter, G. Sguazzoni, W. Tejessy, F. Teubert, A. Valassi, I. Videau, J.J. Ward

European Laboratory for Particle Physics (CERN), CH-1211 Geneva 23, Switzerland

F. Badaud, S. Dessagne, A. Falvard,[20] D. Fayolle, P. Gay, J. Jousset, B. Michel, S. Monteil, D. Pallin, J.M. Pascolo, P. Perret

Laboratoire de Physique Corpusculaire, Université Blaise Pascal, IN²P³-CNRS, Clermont-Ferrand, F-63177 Aubière, France

J.D. Hansen, J.R. Hansen, P.H. Hansen, B.S. Nilsson, A. Wäänänen

Niels Bohr Institute, 2100 Copenhagen, DK-Denmark[9]

A. Kyriakis, C. Markou, E. Simopoulou, A. Vayaki, K. Zachariadou

Nuclear Research Center Demokritos (NRCD), GR-15310 Attiki, Greece

A. Blondel,[12] J.-C. Brient, F. Machefert, A. Rougé, M. Swynghedauw, R. Tanaka H. Videau

Laboratoire de Physique Nucléaire et des Hautes Energies, Ecole Polytechnique, IN²P³-CNRS, F-91128 Palaiseau Cedex, France

V. Ciulli, E. Focardi, G. Parrini

Dipartimento di Fisica, Università di Firenze, INFN Sezione di Firenze, I-50125 Firenze, Italy

A. Antonelli, M. Antonelli, G. Bencivenni, G. Bologna,[4] F. Bossi, P. Campana, G. Capon, V. Chiarella, P. Laurelli, G. Mannocchi,[5] F. Murtas, G.P. Murtas, L. Passalacqua, M. Pepe-Altarelli,[25] P. Spagnolo

Laboratori Nazionali dell'INFN (LNF-INFN), I-00044 Frascati, Italy

J. Kennedy, J.G. Lynch, P. Negus, V. O'Shea, D. Smith, A.S. Thompson

Department of Physics and Astronomy, University of Glasgow, Glasgow G12 8QQ,United Kingdom[10]

S. Wasserbaech

　　Department of Physics, Haverford College, Haverford, PA 19041-1392, U.S.A.

R. Cavanaugh, S. Dhamotharan, C. Geweniger, P. Hanke, V. Hepp, E.E. Kluge, G. Leibenguth, A. Putzer,
H. Stenzel, K. Tittel, S. Werner,[19] M. Wunsch[19]

　　Kirchhoff-Institut für Physik, Universität Heidelberg, D-69120 Heidelberg, Germany[16]

R. Beuselinck, D.M. Binnie, W. Cameron, G. Davies, P.J. Dornan, M. Girone,[1] R.D. Hill, N. Marinelli, J. Nowell,
H. Przysiezniak,[2] S.A. Rutherford, J.K. Sedgbeer, J.C. Thompson,[14] R. White

　　Department of Physics, Imperial College, London SW7 2BZ, United Kingdom[10]

V.M. Ghete, P. Girtler, E. Kneringer, D. Kuhn, G. Rudolph

　　Institut für Experimentalphysik, Universität Innsbruck, A-6020 Innsbruck, Austria[18]

E. Bouhova-Thacker, C.K. Bowdery, D.P. Clarke, G. Ellis, A.J. Finch, F. Foster, G. Hughes, R.W.L. Jones,
M.R. Pearson, N.A. Robertson, M. Smizanska

　　Department of Physics, University of Lancaster, Lancaster LA1 4YB, United Kingdom[10]

V. Lemaitre
　　Institut de Physique Nucléaire, Département de Physique, Université Catholique de Louvain, 1348
　　Louvain-la-Neuve, Belgium

U. Blumenschein, F. Hölldorfer, K. Jakobs, F. Kayser, K. Kleinknecgt, A.-S. Müller, G. Quast,[6] B. Renk,
H.-G. Sander, S. Schmeling, H. Wachsmuth, C. Zeitnitz, T. Ziegler

　　Institut für Physik, Universität Mainz, D-55099 Mainz, Germany[16]

A. Bonissent, J. Carr, P. Coyle, C. Curtil, A. Ealet, D. Fouchez, O. Leroy, T. Kachelhoffer, P. Payre, D. Rousseau,
A. Tilquin
　　Centre de Physique des Particules de Marseille, Univ Méditerranée, IN²P³-CNRS, F-13288 Marseille,
　　France

F. Ragusa
　　Dipartimento di Fisica, Università di Milano e INFN Sezione di Milano, I-20133 Milano, Italy.

A. David, H. Dietl, G. Ganis,[27] K. Hüttmann, G. Lütjens, C. Mannert, W. Männer, H.-G. Moser, R. Settles,
G. Wolf
　　Max-Planck-Institut für Physik, Werner-Heisenberg-Institut, D-80805 München, Germany[16]

J. Boucrot, O. Callot, M. Davier, L. Duflot, J.-F. Grivaz, Ph. Heusse, A. Jacholkowska,[20] C. Loomis, L. Serin,
J.-J. Veillet, J.-B. de Vivie de Régie,[28] C. Yuan
　　Laboratoire de l'Accélérateur Linéaire, Université de Paris-Sud, IN²P³-CNRS, F-91898 Orsay Cedex,
　　France

G. Bagliesi, T. Boccali, L. Foà, A. Giammanco, A. Giassi, F. Ligabue, A. Messineo, F. Palla, G. Sanguinetti,
A. Sciabà, R. Tenchini,[1] A. Venturi,[1] P.G. Verdini
　　Dipartimento di Fisica dell'Università, INFN Sezione di Pisa, e Scuola Normale Superiore, I-56010
　　Pisa, Italy

O. Awunor, G.A. Blair, J. Coles, G. Cowan, A. Garcia-Bellido, M.G. Green, L.T. Jones, T. Medcalf, A. Misiejuk,
J.A. Strong, P. Teixeira-Dias
　　Department of Physics, Royal Holloway & Bedford New College, University of London, Egham, Surrey
　　TW20 OEX, United Kingdom[10]

R.W. Clifft, T.R. Edgecock, P.R. Norton, I.R. Tomalin
　　Particle Physics Dept., Rutherford Appleton Laboratory, Chilton, Didcot, Oxon OX11 OQX, United
　　Kingdom[10]

B. Bloch-Devaux, D. Boumediene, P. Colas, B. Fabbro, E. Lançon, M.-C. Lemaire, E. Locci, P. Perez, J. Rander,
J.-F. Renardy, A. Rosowsky, P. Seager,[13] A. Trabelsi,[21] B. Tuchming, B. Vallage
　　CEA, DAPNIA/Service de Physique des Particules, CE-Saclay, F-91191 Gif-sur-Yvette Cedex,
　　France[17]

N. Konstantinidis, A.M. Litke, G. Taylor

Institute for Particle Physics, University of California at Santa Cruz, Santa Cruz, CA 95064, USA[22]

C.N. Booth, S. Cartwright, F. Combley,[4] P.N. Hodgson, M. Lehto, L.F. Thompson

Department of Physics, University of Sheffield, Sheffield S3 7RH, United Kingdom[10]

K. Affholderbach,[23] A. Böhrer, S. Brandt, C. Grupen, J. Hess, A. Ngac, G. Prange, U. Sieler

Fachbereich Physik, Universität Siegen, D-57068 Siegen, Germany[16]

C. Borean, G. Giannini

Dipartimento di Fisica, Università di Trieste e INFN Sezione di Trieste, I-34127 Trieste, Italy

H. He, J. Putz, J. Rothberg

Experimental Elementary Particle Physics, University of Washington, Seattle, WA 98195 U.S.A.

S.R. Armstrong, K. Berkelman, K. Cranmer, D.P.S. Ferguson, Y. Gao,[29] S. González, O.J. Hayes, H. Hu, S. Jin, J. Kile, P.A. McNamara III, J. Nielsen, Y.B. Pan, J.H. von Wimmersperg-Toeller, W. Wiedenmann, J. Wu, Sau Lan Wu, X. Wu, G. Zobernig

Department of Physics, University of Wisconsin, Madison, WI 53706, USA[11]

G. Dissertori

Institute for Particle Physics, ETH Hönggerberg, 8093 Zürich, Switzerland.

1   Introduction

In the minimal supersymmetric extensions of the Standard Model (MSSM) [1], it is usually assumed that R-parity, $R_p = (-1)^{3B+L+2S}$, is conserved [2]. Here B denotes the baryon number, L the lepton number and S the spin of a field. The conservation of R-parity is not required theoretically and models in which R-parity is violated can be constructed which are compatible with existing experimental constraints.

The R-parity violating terms of the superpotential [3] include a lepton violating contribution $\lambda_{ijk} L_i L_j \bar{E}_k$, where $L_{i(j)}$ are the lepton doublet superfields, $\bar{E}_k$ is the lepton singlet superfield, and λ_{ijk} is the Yukawa coupling corresponding to a particular choice of generational indices i, j, k. A nonzero value for λ_{ijk} implies that the lightest supersymmetric particle (LSP) is not stable and that sparticles could be produced singly. In particular, single sneutrino production would be possible in $\mathrm{e}^+\mathrm{e}^-$ collisions via the $\mathrm{e}\gamma \rightarrow \tilde{\nu}_j \ell_k$ subprocess. For this process, the kinematic reach is typically twice that of pair production. As the production cross section depends on the value of the Yukawa coupling, an observation of supersymmetry in this channel would allow the Yukawa coupling to be directly measured.

In this paper, the results of searches for single sneutrino production via the $\mathrm{e}\gamma \rightarrow \tilde{\nu}_j \ell_k$ subprocess in the data recorded by the ALEPH detector at LEP are reported, under the assumption of a single dominant λ coupling and degenerate sneutrino masses. The paper is organised as follows. In Section 2, the production and decay of single sneutrinos are discussed. In Section 3, the ALEPH detector is briefly described. The details of the data used, the simulation of the signal and the various Standard Model backgrounds are given in Section 4. In Section 5, the selections for the various final states are discussed. Finally, the results are given and the corresponding limits on the λ couplings are presented in Section 6.

2   Single Sneutrino Production and Decay

The tree-level Feynman diagrams for the production of a single sneutrino, via the $\mathrm{e}\gamma \rightarrow \tilde{\nu}_j \ell_k$ subprocess, in $\mathrm{e}^+\mathrm{e}^-$ interactions are shown in Fig. 1. As indicated in Fig. 2, the sneutrino can decay *directly*, $\tilde{\nu} \rightarrow \mathrm{e}\ell$ or, if the neutralino mass is lower than that of the sneutrino, *indirectly* via the lightest neutralino, $\tilde{\nu} \rightarrow \nu\chi$. The possibility of indirect decays via higher mass neutralinos or charginos is not considered in this paper. For small λ couplings, the indirect decays normally dominate over the direct decay, if accessible. The situation is reversed for large λ couplings or small mass differences between the sneutrino and the neutralino. These two extreme configurations are addressed in turn in the following.

The production cross section [4] depends on the assumed value of λ, the mass of the sneutrino, the mass of the lepton produced in association with the sneutrino and the centre-of-mass energy. Figure 3 shows the cross section for $\mathrm{e}^+\mathrm{e}^- \rightarrow \mathrm{e}\mu\tilde{\nu}$ as a function of the sneutrino mass, for two different centre-of-mass energies, and assuming $\lambda_{122(132)} = 0.03$. The cross section for $\mathrm{e}^+\mathrm{e}^- \rightarrow \mathrm{e}\tau\tilde{\nu}$ is about a factor two lower. In the calculation of the cross section, it is assumed that the deflection angle of the beam electron is less than $30\,\mathrm{mrad}$, implying that the electron remains in the beam pipe and is not observed in the detector.
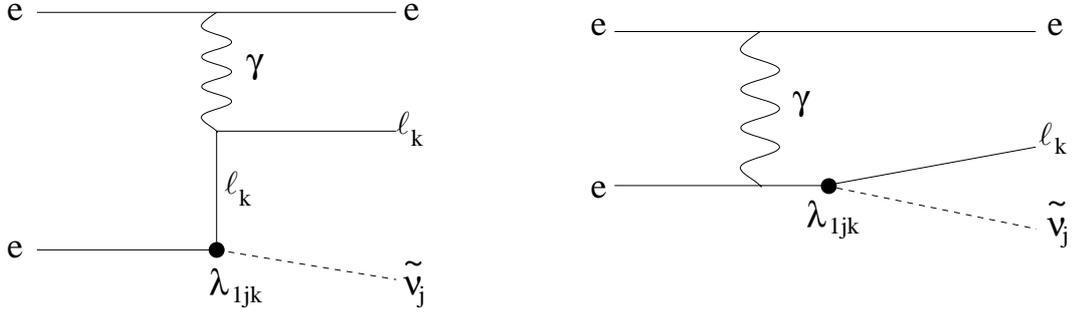
Figure 1: Production of a single sneutrino via the e$\gamma \to \tilde{\nu}_j \ell_k$ subprocess. The $LL\bar{E}$ R-parity violating vertex is indicated by the black dot.
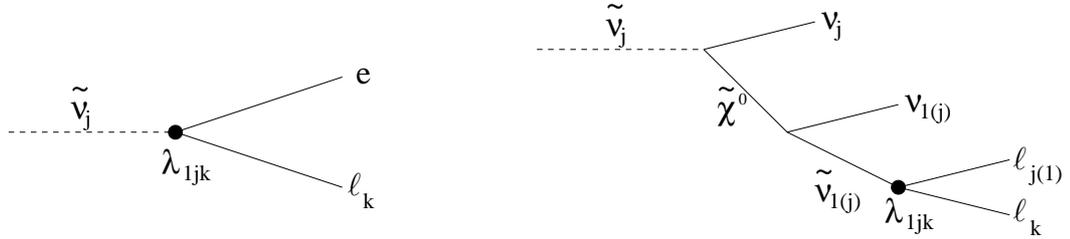
Figure 2: R-parity violating sneutrino decays: (left) direct decay, (right) indirect decay via a neutralino. The $LL\bar{E}$ R-parity violating vertex is indicated by the black dot.

With this production process a sneutrino can be produced via seven of the nine possible λ couplings. Throughout this analysis, only one nonzero λ coupling is assumed, thus the sneutrino is also assumed to decay via the same coupling. A summary of the possible final states corresponding to the seven accessible couplings is shown in Table 1. All the direct and indirect decays, except those for the 121 and 131 couplings, are addressed in the following. For these two couplings the ALEPH search for resonant sneutrino production [5] already provides stringent limits, which cannot be improved upon with the current analysis. For the decay of the neutralino, it is assumed that the sneutrinos are degenerate in mass, leading to two possible decays of equal probability.

3   The ALEPH Detector

The ALEPH detector is described in detail in Ref. [6]. An account of the performance of the detector and a description of the standard analysis algorithms can be found in Ref. [8]. Here, only a brief description of the detector components and the algorithms relevant for this analysis is given.

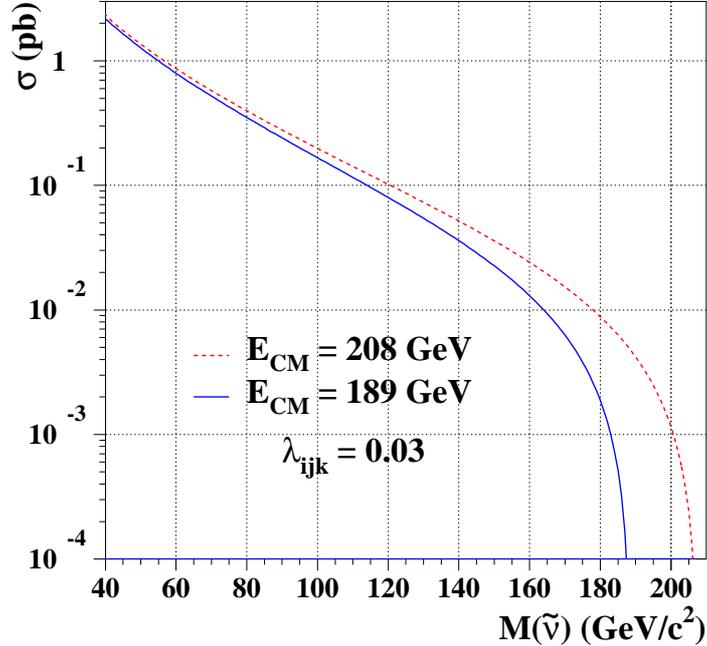**Figure 3:** The cross section for single sneutrino production, assuming $\lambda_{122(132)} = 0.03$, as a function of the sneutrino mass. The full curve is the cross section at a centre-of-mass energy of 189 GeV and the dashed curve is the cross section at a centre-of-mass energy of 208 GeV.

Table 1: The final states produced by the different sneutrino flavours for the various couplings for the direct decays and the indirect decays to the lightest neutralino. The last two leptons listed in the final state are the decay products of the sneutrino. The non detected beam electron is not included in the final state. The charge conjugate reaction, in which the beam positron radiates the photon, is also possible but not indicated. The entries marked with a dash are those for which the sneutrino flavour cannot be produced by the coupling in question.

λ ijk	Direct Decays			Indirect Decays			
	$\tilde{\nu}_e$	$\tilde{\nu}_\mu$	$\tilde{\nu}_\tau$	$\tilde{\nu}_e$	$\tilde{\nu}_\mu$	$\tilde{\nu}_\tau$	χ Decay
121	$\mu^+e^+\mu^-$	$e^+e^+e^-$	-	$\mu^+\nu_e\chi$	$e^+\nu_\mu\chi$	-	$\chi \to \nu_\mu e^+e^-$ or $\nu_e e^\pm\mu^\mp$
131	$\tau^+e^+\tau^-$	-	$e^+e^+e^-$	$\tau^+\nu_e\chi$	-	$e^+\nu_\tau\chi$	$\chi \to \nu_\tau e^+e^-$ or $\nu_e e^\pm\tau^\mp$
122	-	$\mu^+e^+\mu^-$	-	-	$\mu^+\nu_\mu\chi$	-	$\chi \to \nu_\mu e^\mp\mu^\mp$ or $\nu_e\mu^+\mu^-$
132	-	-	$\mu^+e^+\mu^-$	-	-	$\mu^+\nu_\tau\chi$	$\chi \to \nu_\tau e^\pm\mu^\mp$ or $\nu_e\mu^\pm\tau^\mp$
123	-	$\tau^+e^+\tau^-$	-	-	$\tau^+\nu_\mu\chi$	-	$\chi \to \nu_\mu e^\pm\tau^\mp$ or $\nu_e\mu^\pm\tau^\mp$
133	-	-	$\tau^+e^+\tau^-$	-	-	$\tau^+\nu_\tau\chi$	$\chi \to \nu_\tau e^\pm\tau^\mp$ or $\nu_e\tau^+\tau^-$
231	-	$\tau^+e^+\tau^-$	$\mu^+e^+\mu^-$	-	$\tau^+\nu_\mu\chi$	$\mu^+\nu_\tau\chi$	$\chi \to \nu_\tau e^\pm\mu^\mp$ or $\nu_\mu e^\pm\tau^\mp$

The trajectories of charged particles are measured with a silicon vertex detector, a cylindrical drift chamber, and a large time projection chamber (TPC). The central detectors

Table 2: Integrated luminosity for all data collected by ALEPH in 1998-2001.

$\sqrt{s}$	189 GeV	192 GeV	196 GeV	200-202 GeV	203-209 GeV
Luminosity	$174.2\,\mathrm{pb}^{-1}$	$28.9\,\mathrm{pb}^{-1}$	$78.8\,\mathrm{pb}^{-1}$	$128.2\,\mathrm{pb}^{-1}$	$227.0\,\mathrm{pb}^{-1}$

are immersed in a 1.5 T axial magnetic field provided by a superconducting solenoidal coil. The electromagnetic calorimeter (ECAL), placed between the TPC and the coil, is a highly segmented sampling calorimeter which is used to identify electrons and photons and to measure their energies. The luminosity monitors extend the calorimetric coverage down to 34 mrad from the beam axis. The hadron calorimeter (HCAL) consists of the iron return yoke of the magnet instrumented with streamer tubes. It provides a measurement of hadronic energy and, together with the external muon chambers, muon identification. The calorimetric and tracking information are combined in an energy flow algorithm which provides a list of charged and neutral objects. It also gives a measure of the total visible energy, and therefore the missing energy.

Electron identification is primarily based upon the matching between the measured momentum of the charged track and the energy deposited in the ECAL. Additional information from the shower profile in the ECAL is also used. To take into account energy loss due to bremsstrahlung and/or final state radiation photons, the sum of the ECAL energy deposits within a 5° cone centred on the impact point of an isolated electron is added to the energy determined by the tracking, if the additional energy is greater than 300 MeV.

Muons are separated from hadrons by their characteristic pattern in the HCAL and the presence of associated hits in the muon chambers. A correction for final state radiation photons, similar to that used for the electrons, is also applied. In this case, the additional ECAL energy is only used if greater than 2 GeV.

4   Data and Monte Carlo Samples

This analysis was performed using data collected with the ALEPH detector during 1998-2001. It corresponds to an integrated luminosity of $637.1\,\mathrm{pb}^{-1}$ at centre-of-mass energies from 189 up to 209 GeV (Table 2).

The signal was simulated with SUSYGEN [9], modified to include single sneutrino production. Final state radiation was implemented using PHOTOS [10] and tau decays via TAUOLA [11]. The events were passed through the full simulation chain of the ALEPH detector and the reconstruction program applied to the data.

Monte Carlo samples simulating all relevant Standard Model processes were used, corresponding to at least 100 times the collected luminosity in the data, except for the process $\gamma\gamma \to$ leptons where 10 million events were generated, corresponding to more than six times the collected luminosity in the data. Events from $e^+e^- \to q\bar{q}$ at 189 GeV and four-fermion events from Weν, ZZ and Zee were produced with PYTHIA [12]. The process $e^+e^- \to q\bar{q}$ above 189 GeV was produced with KORALZ [13]. Pairs of W bosons were generated with KORALW [14]. Pair production of leptons was simulated with BHWIDE [15] (electrons) and KORALZ [13] (muons and taus), and the two-photon processes with PHOT02 [16].

5 Event Selections

The signal is characterised by a charged lepton, the decay products of the sneutrino and missing energy from an electron lost in the beam pipe. The flavours of the three final state leptons depend on the coupling involved. In the case of indirect decays and decays involving taus, there can be significant additional missing momentum, of no particular preferred direction, due to the presence of neutrinos in the final state.

A number of selections were developed to select the final states listed in Table 1 from the Standard Model backgrounds. As sneutrinos with masses less than $82\,\mathrm{GeV}/c^2$ for a $\lambda > 10^{-7}$ are already excluded by the pair production search [5], the selections were optimised to give the minimum expected 95% C.L. excluded cross section [17] for sneutrino masses above $80\,\mathrm{GeV}/c^2$. For the indirect decays, mass differences between the sneutrino and neutralino less than $5\,\mathrm{GeV}/c^2$ were not considered. Neutralino masses less than $20\,\mathrm{GeV}/c^2$ were not considered either as they are already excluded [18].

A preselection requiring low charged multiplicity ($N_{\mathrm{ch}} < 6$), at least one identified electron or muon ($N_{\mathrm{e}} + N_{\mu} > 0$), and only a small amount of energy within a $12°$ cone around the beam axis ($E_{12} < 20\,\mathrm{GeV}$), allows most of the hadronic and semileptonic backgrounds to be rejected. The remaining backgrounds are low multiplicity leptonic events.

The acoplanarity angle between jets (acopJet), obtained by forcing the event to form two jets using the Durham algorithm [7], is a powerful tool to reject many of the backgrounds. The Zee and ZZ backgrounds are reduced using an anti-Z mass cut. Various requirements on the angles between the leptons and their angle with respect to the beam axis are also applied. In some cases, sliding cuts are adopted which depend upon the assumed sneutrino mass.

For the direct decays to electron and muon (λ_{122}, λ_{132} and λ_{231}), the invariant mass of the sneutrino can be reconstructed, unlike for the indirect decays and direct decays with a tau in the final state. For these decays, requirements on the fraction of visible energy ($E_{\mathrm{vis}}/\sqrt{s}$), the direction of the missing momentum (θ_{miss}) and the amount of missing transverse momentum (P_{T}) are applied.

The various selections are outlined below and summarized in the Tables of the Appendix.

5.1 Direct Decay via λ_{122} or λ_{132}

The direct sneutrino decays via λ_{122} and λ_{132} differ only in the flavour of the intermediate sneutrino produced. The decay products from the sneutrino ($e^+\mu^-$) and the complete final state ($e^+\mu^-\mu^+$) are identical for both couplings.

The complete set of selection cuts is listed in Table A1. The selection requires one and only one identified electron in the event (N_{e}), and that the angle θ_{e} of this electron with respect to the beam axis be large. In addition, it is required that the visible energy fraction be significant and that the total transverse momentum of the event be small.

As in about 20% of the cases a second lepton (in addition to the beam electron) is outside the tracking acceptance, the selection treats the case of two or three charged particles separately. For the two track case, it is required that the other track be an identified muon of opposite

charge to the electron and that the electron and muon be not back-to-back ($\theta_{\mathrm{e}\mu}$). For the three track case, at least one muon has to be identified. In addition, the muon and the non-electron track must not be back-to-back ($\theta_{\mu\mathrm{t}}$), and the invariant mass $M_{\mu\mathrm{t}}$ of these two tracks must be inconsistent with the Z mass. Figure 4 shows the Z $\rightarrow \mu^+\mu^-$ mass peak obtained in data compared with Monte Carlo expectations, after applying the preselection.

The efficiency of the complete selection increases from 25% for a sneutrino mass of $60\,\mathrm{GeV}/c^2$ to 55% for a sneutrino mass of $180\,\mathrm{GeV}/c^2$. Summing over all centre-of-mass energies a total of 38 events is observed in the data while 46.7 are expected from Standard Model backgrounds. Figure 5 shows the $\mathrm{e}^+\mu^-$ mass distribution of the selected events. As indicated in the figure, a signal would produce a peak centred around the mass of the sneutrino. For the extraction of the λ exclusions , events are counted within a mass window of variable width which is scanned across this $\mathrm{e}^+\mu^-$ mass distribution.

5.2 Direct Decay via λ_{123} or λ_{133}

The direct sneutrino decays via λ_{123} and λ_{133} differ only in the flavour of the intermediate sneutrino produced. The decay products from the sneutrino ($\mathrm{e}^+\tau^-$) and the complete final state ($\mathrm{e}^+\tau^-\tau^+$) are identical for both couplings.

The complete set of selection cuts is listed in Table A2. For the two tau's, the 1/1 and 1/3 prong decays are considered, leading to a final state with three or five charged particles. The tau decays into electrons and muons are considered in the requirements on the numbers of electrons and muons in the event. As the events contain neutrinos from the tau decays, a large transverse momentum and significant missing energy are required . The missing momentum is also required not to be in the direction of the beam axis.

The most energetic electron in the event, usually produced directly from the sneutrino decay, is required to have an energy E_{emax} greater than $20\,\mathrm{GeV}$ and the direction of this electron θ_{emax} is required to be away from the beam axis.

The assignment of the charged and neutral objects to the two taus is performed by removing the most energetic electron from the event. Requirements are made that the tau "jets" have opposite charge and be not back-to-back ($\theta_{\tau_1\tau_2}$). Additional requirements on the transverse momentum of the most energetic tau jet ($P_{\mathrm{T(maxEjet)}}$) and the angle between the most energetic electron and the same sign tau jet ($\theta_{\mathrm{emax}^\pm/\tau^\pm}$) are also applied.

After all selection criteria, the efficiency for the signal rises from 15% for a sneutrino mass of $60\,\mathrm{GeV}/c^2$ to 35% for a $160\,\mathrm{GeV}/c^2$ sneutrino. A total of 13 events is selected in the data, consistent with the 17.1 events expected from the Standard Model backgrounds. Due to the presence of neutrinos in its decay, the mass of the sneutrino cannot be directly reconstructed from the decay products. Nevertheless, the energy of the most energetic electron and the angle between this electron and the opposite-sign tau ($\theta_{\mathrm{emax}^\pm/\tau^\mp}$) are sensitive to the sneutrino mass. These variables are therefore used to establish sliding cuts for extraction of the λ exclusions. Figure 6 shows the distribution of $\theta_{\mathrm{emax}^\pm/\tau^\mp}$ in the data, after the preselection, compared to Monte Carlo expectations.

6

5.3 Direct Decay via λ_{231}

The direct decay via the λ_{231} coupling can proceed via two different flavours of sneutrino. The production of a $\tilde{\nu}_\tau$ leads to a final state with two muons and an electron. The decay via a $\tilde{\nu}_\mu$ leads to a final state with two taus and an electron. Due to the mass of the tau produced in association with the $\tilde{\nu}_\mu$, this channel is suppressed by a factor 2.25 with respect to the $\tilde{\nu}_\tau$ channel.

As the final states are identical to those for the direct decays via the λ_{1j2} and λ_{1j3} couplings, previously discussed, no additional selection was developed for this coupling.

5.4 Indirect Decay via λ_{122}

Depending on the neutralino decay, the indirect decay via the λ_{122} coupling can produce two distinct final states of equal probability, either two muons and an electron plus neutrinos or three muons plus neutrinos.

For the selection (Table A3), three charged tracks are required of which at least two must be identified as muons. Cuts requiring a large transverse momentum in the event and a large missing momentum not pointing along the beam axis are used. Figure 8 shows the distrbution of the missing P_T at the preselection level. For the case of three identified muons, a cut removing combinations consistent with the Z mass, is used to reject the ZZ background. For the case of two identified muons an additional cut requiring the polar angle of the non-muon track (θ_t) to be away from the beam axis is applied.

The efficiency of the selection for the signal varies between 40% and 50% and is insensitive to the mass of the neutralino involved in the decay. No event is selected in the data, consistent with the Standard Model background expectation of 2.1 events.

5.5 Indirect Decay via λ_{132}

Depending on the neutralino decay, the indirect decay via the λ_{132} coupling can produce two distinct final states of equal probability, either two muons and an electron plus neutrinos or two muons and a tau plus neutrinos.

For the selection (Table A4) only the one-prong decays of the tau are considered. Three charged tracks are therefore required, of which at least one must be identified as a muon. Only one identified electron is allowed in the event. Cuts requiring a large transverse momentum and a large missing energy whose direction is away from the beam axis are also applied. A cut on the acoplanarity of two jets is also used.

The efficiency of the selection for the signal is 30%–40% depending on the sneutrino mass and is insensitive to the mass of the neutralino involved in the decay. Three events are selected in the data, consistent with the Standard Model background expectation of 2.2 events.

5.6 Indirect Decay via λ_{123}

Depending on the neutralino decay, the indirect decay via the λ_{123} coupling can produce two distinct final states of equal probability, either two taus with an electron or two taus with a muon.

The complete list of selection criteria can be found in Table A5. A total of three or five charged particles is required in the event, corresponding to the case where the two taus decay into 1/1 prong or 1/3 prongs. Due to the presence of neutrinos in each of the sneutrino, neutralino and tau decays, this channel is characterised by a small visible energy and large transverse momentum.

Cuts on the acoplanarity angle (acopJet) between the two jets, the transverse momentum ($P_{T(maxEjet)}$) of the most energetic jet , and the angle θ_{jet_1,jet_2} between the two jets are effective at reducing the backgrounds from $\gamma\gamma \rightarrow \tau^+\tau^-$ and $Z \rightarrow \tau^+\tau^-$. Figure 7 shows the distribution of acopJet at the preselection level. Finally a cut on y_{23}, the Durham distance for the transition from two to three jets, is applied to reject $\gamma\gamma \rightarrow \ell^+\ell^-$ and $e^+e^- \rightarrow \ell^+\ell^-$.

The efficiency of this selection for the signal rises from 25% for a sneutrino mass of $60\,\text{GeV}/c^2$ to 40% for a sneutrino mass of $180\,\text{GeV}/c^2$. The dependence of the efficiency on the neutralino mass is small. A total of 14 events is selected in the data, consistent with the 14.9 events expected from the Standard Model backgrounds.

5.7 Indirect Decay via λ_{133}

Depending on the neutralino decay, the indirect decay via the λ_{133} coupling can produce two distinct final states of equal probability, either two taus and an electron plus neutrinos or three taus plus neutrinos. These events are therefore characterised by a large number of taus in the final state.

The selection is summarised in Table A6. Three or five charged tracks are demanded, implying that the 1/1 and 1/3 prong decays of the two taus are considered in the two-tau final state (97.5% of the cases), and the 1/1/1 and 1/1/3 prong decays are considered for the three-tau final state (93.5% of the cases). Up to two identified electrons or muons are allowed in the event. Due to the presence of neutrinos, cuts requiring a large transverse momentum and a large missing momentum not pointing along the beam axis are applied. A cut on the acoplanarity of the event is also used. For the case of three charged tracks the backgrounds are larger than the five-track case, necessitating tighter cuts.

The efficiency of the selection for the signal is 20%–35%, depending on the sneutrino mass and is insensitive to the mass of the neutralino involved in the decay. A total of 16 events is selected in the data, consistent with the Standard Model background expectation of 16.6 events.

5.8 Indirect Decay via λ_{231}

The production and indirect decay of sneutrinos via the λ_{231} coupling lead to different final states depending on whether a $\tilde{\nu}_\mu$ or a $\tilde{\nu}_\tau$ is produced and on the subsequent decay of the

Table 3: The selection efficiency, the numbers of expected background and the numbers of observed events for each selection (any sliding cuts removed) summed over all centre-of-mass energies.

Selection	Efficiency (%)	Expected Background	Observed Data
$1j2$ direct	$25 \rightarrow 55$	46.7	38
$1j3$ direct	$15 \rightarrow 35$	17.1	13
123 indirect	$25 \rightarrow 40$	14.9	14
122 indirect	$40 \rightarrow 50$	2.1	0
132 indirect	$30 \rightarrow 40$	2.2	3
231 indirect	$25 \rightarrow 45$	10.1	9
133 indirect	$20 \rightarrow 35$	16.6	16

neutralino. Taking into account the different production cross sections of the two sneutrino flavours, the relative probabilities of each final state are 15.4% $\tau\tau$e, 34.6% $\tau\mu$e and 50% $\mu\mu$e.

The selection (Table A7) treats the final states globally and only considers the one-prong decays of the tau. The simultaneous presence of an electron and a muon ($\sim 85\%$ of the cases) in the event, associated with a large amount of missing energy and acoplanarity, allows most of the backgrounds to be rejected.

The efficiency of the selection varies between 25% and 45%, depending on the sneutrino mass, and is insensitive to the neutralino mass involved in the decay. A total of nine events is selected in the data, while 10.1 are predicted from Standard Model backgrounds.

6 Results and Upper Limits on the λ Couplings

The numbers of observed and expected events, obtained after applying the various selections (except the sliding cuts), are summarised in Table 3. The observed numbers are in good agreement with the Standard Model expectations, indicating no evidence for single sneutrino production. Upper limits on the values of the various $LL\bar{E}$ couplings are therefore derived.

In the calculation of the limits, background subtraction was performed for the two- and four-fermion final states. The uncertainties on the background estimates were taken into account by reducing the amount of background subtracted. For the two-fermion processes, the amount of background subtracted was reduced by its Monte Carlo statistical uncertainty. The backgrounds subtracted for the four-fermion processes were reduced by 20% of their estimate. The $\gamma\gamma \rightarrow f\bar{f}$ background was not subtracted.

The systematic uncertainties on the selection efficiencies are 4–5%, dominated by the signal Monte Carlo statistical uncertainty, with small additional contributions from the simulation of lepton identification and energy flow reconstruction. These uncertainties were conservatively taken into account by reducing the selection efficiencies by one standard deviation.

Possible differences between the data and the simulation in the distribution of the E_{12} variable, due to the presence of beam-related backgrounds in the data, were investigated using events triggered at random beam crossing. The difference between data and Monte Carlo in

Table 4: The 95% CL upper limits obtained on the various λ couplings assuming a sneutrino mass of $100\,\mathrm{GeV}/c^2$. The last column shows the corresponding low energy bounds [19]. In parentheses are indicated the sneutrino mass up to which these analyses improve upon the low energy bounds.

λ Coupling	95% CL Upper Limit		
	Direct Decay	Indirect Decay	Low Energy Bound
122	0.014 $(189\,\mathrm{GeV}/c^2)$	0.007 $(190\,\mathrm{GeV}/c^2)$	0.04
123	0.028 $(174\,\mathrm{GeV}/c^2)$	0.025 $(147\,\mathrm{GeV}/c^2)$	0.04
132	0.014 $(191\,\mathrm{GeV}/c^2)$	0.012 $(187\,\mathrm{GeV}/c^2)$	0.05
133	0.028 $(\quad - \quad)$	0.029 $(\quad - \quad)$	0.003
231	0.014 $(191\,\mathrm{GeV}/c^2)$	0.016 $(189\,\mathrm{GeV}/c^2)$	0.05

the fraction of energy deposits in the forward detectors, when this energy is less than $20\,\mathrm{GeV}$, was found to be less than 5 per mill.

The Zee background, with $\mathrm{Z} \to \mu^+\mu^-$, proceeds via a similar production mechanism and has the same final state as a sneutrino with a mass equal to the Z decaying directly through a λ_{1j2} coupling, except that the electron in the sneutrino decay is replaced by a muon. As a check of the analysis procedure, the λ_{1j2} selection was therefore modified to select the Zee background. Figure 9 shows the $\mu^+\mu^-$ mass spectrum after applying the modified selection. A clear peak around the Z mass is observed, consistent with expectations from the Zee and the two-fermion $\mu\mu$ simulations.

As the cross section for sneutrino production is a function of λ and the sneutrino mass, the corresponding 95% confidence level exclusions are presented in the λ versus $M_{\tilde{\nu}}$ plane in Figs. 10 to 14. Also indicated on these figures are the exclusions obtained by the ALEPH search for pair production of sneutrinos decaying via a $LL\bar{E}$ coupling [5] and the low energy bounds [19].

Table 4 compares the 95% CL upper limits obtained on the couplings (direct and indirect decays), for an assumed sneutrino mass of $100\,\mathrm{GeV}/c^2$, with the low energy bounds. Except for the λ_{133} coupling, which already has a stringent upper limit from the ν_{e} mass constraint, significantly improved upper limits are obtained on the other couplings for sneutrino masses up to $\sim 190\,\mathrm{GeV}/c^2$.

7   Summary

A number of searches sensitive to R-parity violating production and decay of single sneutrinos have been presented. These searches find no evidence for R-parity violated supersymmetry in the ALEPH data collected at $\sqrt{s} = 189$ to $209\,\mathrm{GeV}$. Within the framework of the MSSM, assuming that a single λ coupling dominates and that the sneutrinos are degenerate in mass, limits on the various λ couplings as a function of the assumed sneutrino mass have been derived. These searches improve by up to a factor five upon the existing 95% CL upper limits on four of the λ couplings for sneutrino masses up to $190\,\mathrm{GeV}/c^2$, and are valid independent of whether the sneutrino decays directly or via the lightest neutralino. This paper is the first publication of such an analysis at LEP.

8 Acknowledgements

It is a pleasure to congratulate our colleagues from the accelerator divisions for the successful operation of LEP at high energy. We would like to express our gratitude to the engineers and support people at our home institutes without whose dedicated help this work would not have been possible. Those of us from non-member states wish to thank CERN for its hospitality and support.

References

[1] For reviews, see for example:
    H.P. Nilles, Phys. Rep. **110** (1984) 1;
    H.E. Haber and G. L. Kane, Phys. Rep. **117** (1985) 75.

[2] G. Farrar and P. Fayet, Phys. Lett. **B 76** (1978) 575.

[3] S. Weinberg, Phys. Rev. **B 26** (1982) 287; N. Sakai and T. Yanagida, Nucl. Phys. **B 197** (1982) 83; S. Dimopoulos, S. Raby and F. Wilczek, Phys. Lett. **B 212** (1982) 133.

[4] B.C. Allanach, H. Dreiner, P. Morawitz and M.D. Williams, *"Single Sneutrino/Slepton Production at LEP2 and the NLC"*, Phys. Lett. **B 420** (1998) 307.

[5] ALEPH Collaboration, *"Search for R-Parity Violating Decays of Supersymmetric Particles in e^+e^- Collisions at Centre-of-Mass Energies between $\sqrt{s} = 189$–$202\,GeV$"*, Eur. Phys. J. **C 19** (2001) 415.

[6] ALEPH Collaboration, *"ALEPH: a detector for electron-positron annihilations at LEP"*, Nucl. Instrum. and Methods. **A 294** (1990) 121.

[7] S. Cantini, Yu. L. Dokshitzer, M. Olsson, G. Turnock and B.R. Webber, *'New clustering algorithm for multijet cross sections in e^+e^- annihilation"*, Phys. Lett. **B 269** (1991) 432.

[8] ALEPH Collaboration, *"Performance of the ALEPH detector at LEP"*, Nucl. Instrum. and Methods. **A 360** (1995) 481.

[9] S. Katsanevas and P. Morawitz, *"SUSYGEN 2.2 - A Monte Carlo Event Generator for MSSM Sparticle Production at e^+e^- Colliders"*, Comput. Phys. Commun. **112** (1998) 227.

[10] E. Barberio, B. van Eijk and Z. Wąs, Comput. Phys. Commun. **66** (1991) 115.

[11] S. Jadach and Z. Wąs, R. Decker and J.H. Kühn, *"The τ decay library TAUOLA"*, Comput. Phys. Commun. **76** (1993) 361.

[12] T. Sjöstrand, *" High-Energy Physics Event Generation with PYTHIA 5.7 and JETSET 7.4"* , Comput. Phys. Commun. **82** (1994) 74.

[13] S. Jadach *et al.*, Comput. Phys. Commun. **66** (1991) 276.

[14] M. Skrzypek, S. Jadach, W. Placzek and Z. Was, Comput. Phys. Commun. **94** (1996) 216.

[15] S. Jadach *et al.*, Phys. Lett. **B 390** (1997) 298.

[16] J.A.M. Vermaseren, in *Proceedings of the IVth International Workshop on Gamma Gamma Interactions*, Eds. G. Cochard and P. Kessler, Springer Verlag, 1980.

[17] J. -F. Grivaz and F. Le Diberder, *"Complementary analyses and acceptance optimization in new particle searches"*, LAL preprint # 92-37 (1992).

[18] ALEPH Collaboration, *"Search for Supersymmetry with a dominant R-Parity Violating $LL\bar{E}$ Coupling in e^+e^- Collisions at Centre-of-Mass Energies of $130\,GeV$ to $172\,GeV$"*, Eur. Phys. J. **C 4** (1998) 433.

[19] For reviews see for example:
H. Dreiner, *"An Introduction to Explicit R-parity Violation"*, hep-ph/9707435, published in *Perspectives on Supersymmetry*, ed. G.L. Kane, World Scientific, Singapore (1998);
G. Bhattacharyya, Nucl. Phys. Proc. Suppl. **52A** (1997) 83.

Appendix

Table A1: Selection cuts for direct sneutrino decays via the λ_{122} and λ_{132} couplings.

$E_{\mathrm{vis}}/\sqrt{s} > 50\%$	
$N_{\mathrm{e}} = 1$	
$N_{\mathrm{ch}} = 2$	$N_{\mathrm{ch}} = 3$
$P_{\mathrm{T}} < 8.5\,\mathrm{GeV}/c$	$P_{\mathrm{T}} < 10\,\mathrm{GeV}/c$
$\lvert\cos\theta_{\mathrm{e}}\rvert < 0.8$	$\lvert\cos\theta_{\mathrm{e}}\rvert < 0.9$
$N_{\mu} = 1$, opp. charge to e	$N_{\mu} = 1$ or 2
$\lvert\cos\theta_{\mathrm{e}\mu}\rvert < 0.99$	$\lvert\cos\theta_{\mu\mathrm{t}}\rvert < 0.9$
	$\lvert M_{\mu\mathrm{t}} - M_{\mathrm{Z}}\rvert > 4\,\mathrm{GeV}/c^2$
sliding mass cut: $\lvert M_{\mathrm{e}^{\pm}\mu^{\mp}} - M_{\tilde{\nu}}\rvert < (M_{\tilde{\nu}}/20 - 0.6)\,\mathrm{GeV}/c^2$	

Table A2: Selection cuts for direct sneutrino decays via the λ_{123} and λ_{133} couplings.

$N_{\mathrm{ch}} = 3$ or 5,
$0 < N_{\mathrm{e}} < 3, N_{\mu} < 2$
$P_{\mathrm{T}} > 6\,\mathrm{GeV}/c$
$25\% < E_{\mathrm{vis}}/\sqrt{s} < 90\%$
$\lvert\cos\theta_{\mathrm{miss}}\rvert < 0.98$
$E_{\mathrm{emax}} > 20\,\mathrm{GeV}$
$\lvert\cos\theta_{\mathrm{emax}}\rvert < 0.9$
$2\ \tau$'s with opposite charge
$1/1$ or $1/3$ prongs
$\lvert\cos\theta_{\tau_1\tau_2}\rvert < 0.95$
$P_{\mathrm{T(maxEjet)}} > 5\,\mathrm{GeV}/c$
$\lvert\cos\theta_{\mathrm{emax}^{\pm}/\tau^{\pm}}\rvert > 0.9$
sliding cuts:
$f(M_{\tilde{\nu}}) < \lvert\cos\theta_{\mathrm{emax}^{\pm}/\tau^{\mp}}\rvert < f'(M_{\tilde{\nu}})$
$f''(M_{\tilde{\nu}}) < E_{\mathrm{emax}} < f'''(M_{\tilde{\nu}})$

Table A3: Selection cuts for indirect sneutrino decays via the λ_{122} coupling.

$N_{\mathrm{ch}} = 3$	
$N_{\mu} = 3$	$N_{\mu} = 2$
$P_{\mathrm{T}} > 4\,\mathrm{GeV}/c$	$P_{\mathrm{T}} > 6\,\mathrm{GeV}/c$
$E_{\mathrm{vis}}/\sqrt{s} < 80\%$	$E_{\mathrm{vis}}/\sqrt{s} < 70\%$
$\lvert\cos\theta_{\mathrm{miss}}\rvert < 0.95$	$\lvert\cos\theta_{\mathrm{miss}}\rvert < 0.98$
$\lvert M_{\mu\mu} - M_{\mathrm{Z}}\rvert > 4\,\mathrm{GeV}/c^2$	$\lvert\cos\theta_{\mathrm{t}}\rvert < 0.98$

Table A4: Selection cuts for indirect sneutrino decays via the λ_{132} coupling.

$$
\begin{array}{c}
N_{\text{ch}} = 3 \\
N_{\text{e}} < 2,\ N_{\mu} > 1 \\
P_{\text{T}} > 5\,\text{GeV}/c \\
E_{\text{vis}}/\sqrt{s} < 80\% \\
|\cos\theta_{\text{miss}}| < 0.95 \\
\text{acopJet} < 170°
\end{array}
$$

Table A5: Selection cuts for indirect sneutrino decays via the λ_{123} coupling.

$$
\begin{array}{c}
N_{\text{ch}} = 3\ \text{or}\ 5 \\
N_{\text{e}} + N_{\mu} < 4 \\
P_{\text{T}} > 7\,\text{GeV}/c \\
10\% < E_{\text{vis}}/\sqrt{s} < 60\% \\
|\cos\theta_{\text{miss}}| < 0.9 \\
\text{acopJet} < 170° \\
P_{\text{T(maxEjet)}} > 5\,\text{GeV}/c^2 \\
y_{23} > 2.5\ 10^{-4} \\
|\cos\theta_{\text{jet1,jet2}}| < 0.95
\end{array}
$$

Table A6: Selection cuts for indirect sneutrino decays via the λ_{133} coupling.

$N_{\text{ch}} = 3\ \text{or}\ 5$	
$N_{\text{e}} + N_{\mu} < 3$	
$|\cos\theta_{\text{miss}}| < 0.95$	
$\text{acopJet} < 160°$	
$N_{\text{ch}} = 3$	$N_{\text{ch}} = 5$
$P_{\text{T}} > 10\,\text{GeV}/c$	$P_{\text{T}} > 7\,\text{GeV}/c$
$E_{\text{vis}}/\sqrt{s} < 50\%$	$E_{\text{vis}}/\sqrt{s} < 60\%$
$|\cos\theta_{\text{jet}-\text{jet}}| < 0.9$	

Table A7: Selection cuts for indirect sneutrino decays via the λ_{231} coupling.

$$
\begin{array}{c}
N_{\text{ch}} = 3 \\
N_{\text{e}} > 0,\ N_{\mu} > 0 \\
P_{\text{T}} > 7\,\text{GeV}/c \\
E_{\text{vis}}/\sqrt{s} < 75\% \\
|\cos\theta_{\text{miss}}| < 0.94 \\
\text{acopJet} < 170°
\end{array}
$$
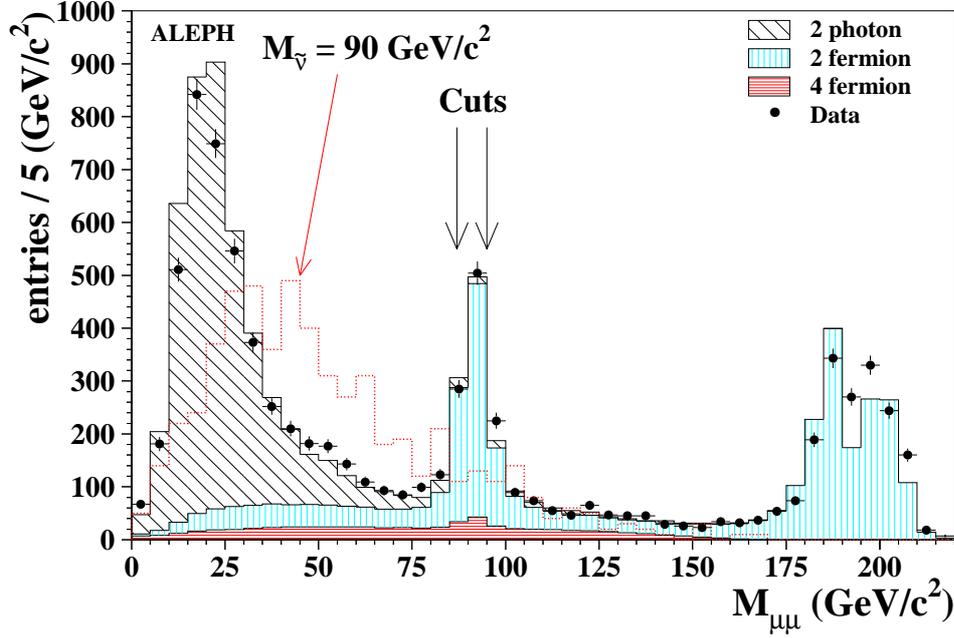
Figure 4: The $\mu^+\mu^-$ invariant mass distribution, obtained after applying the preselection, for $\sqrt{s} = 189$–$209\,\mathrm{GeV}$: data (dots with error bars), expected background (solid histogram). The expected distribution (arbitrary normalisation) for a signal of $M_{\tilde{\nu}} = 90\,\mathrm{GeV}/c^2$ is also indicated (dotted histogram).
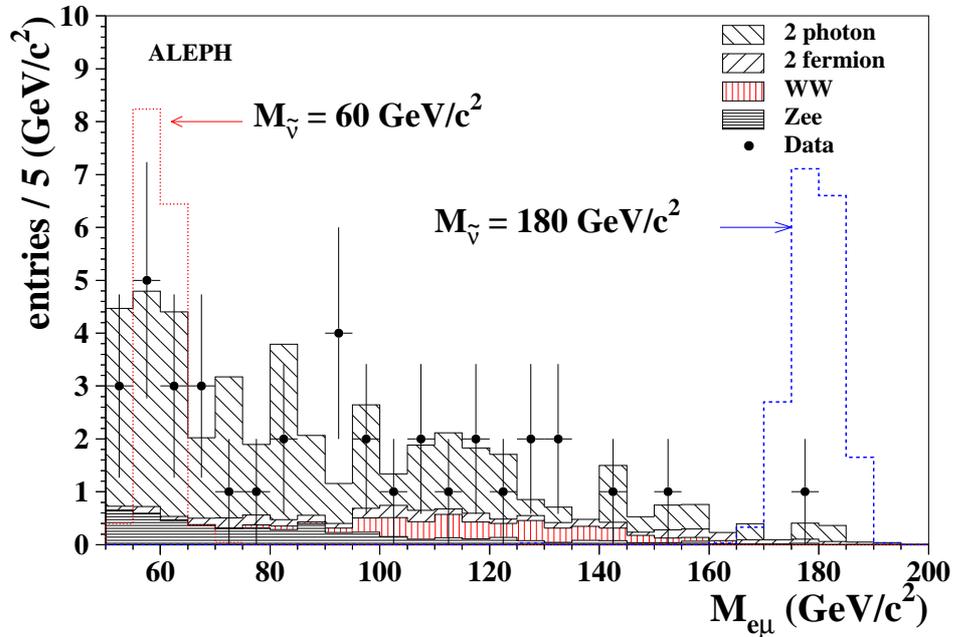

Figure 5: The $e^+\mu^-$ invariant mass distribution, obtained after applying the λ_{1j2} selection, for $\sqrt{s} = 189$–$209\,\mathrm{GeV}$: data (dots with error bars), expected background (solid histogram). The expected distribution ($\lambda = 0.03$) for a signal of $M_{\tilde{\nu}} = 60\,\mathrm{GeV}/c^2$ (dotted histogram) and $M_{\tilde{\nu}} = 180\,\mathrm{GeV}/c^2$ are also indicated (dashed histogram).
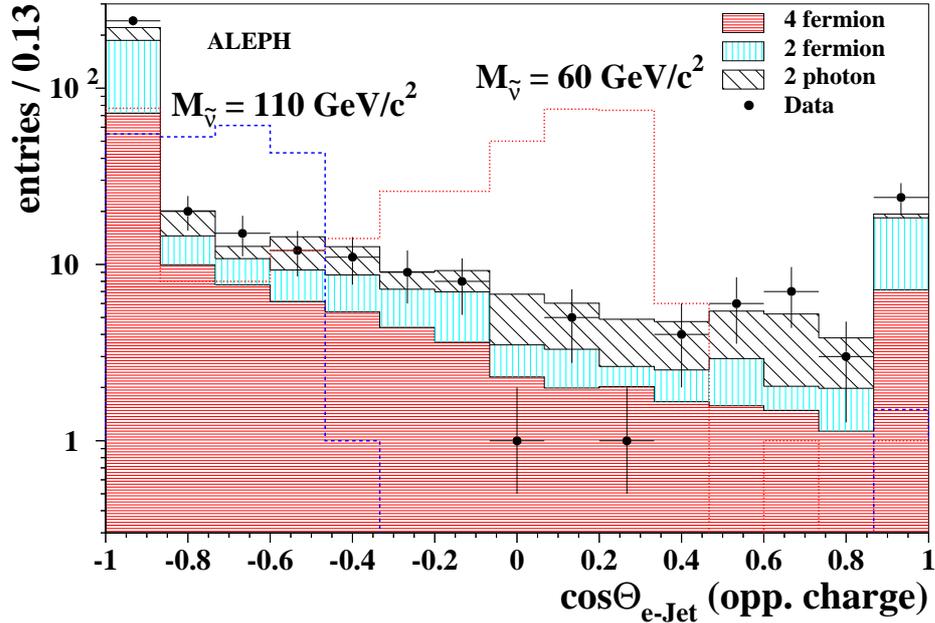
Figure 6: The distribution, at preselection level, of the angle between the most energetic electron and the opposite-sign tau jet, used in the λ_{1j3} selection, for $\sqrt{s} = 189$–209 GeV: data (dots with error bars), expected background (solid histogram). The expected distribution (arbitrary normalisation) for a signal of $M_{\tilde{\nu}} = 60$ GeV/c^2 (dotted histogram) and $M_{\tilde{\nu}} = 160$ GeV/c^2 are also indicated (dashed histogram).
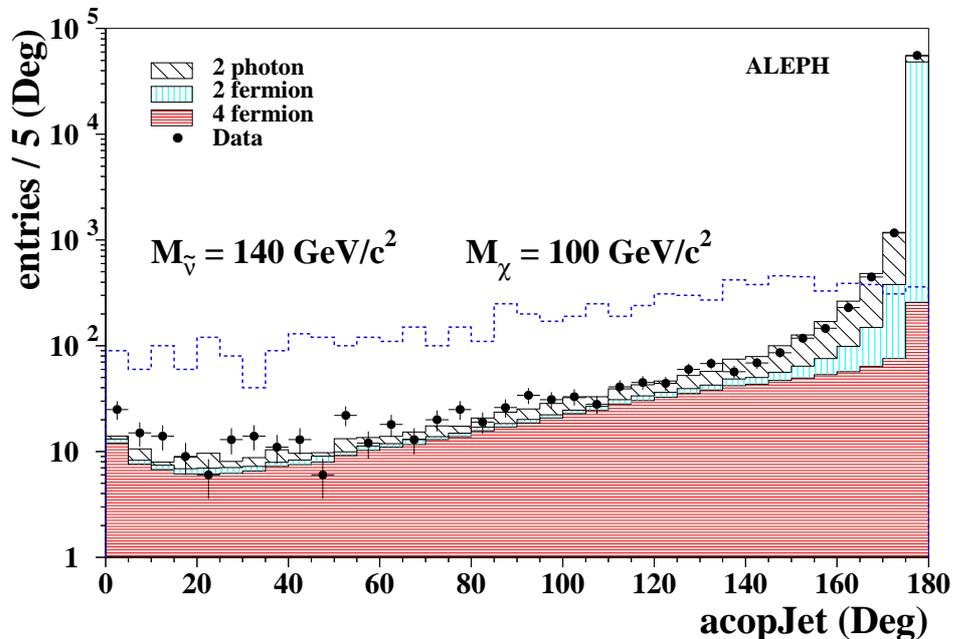
Figure 7: The distribution of the acoplanarity between two jets, at the preselection level, for $\sqrt{s} = 189$–209 GeV: data (dots with error bars), expected background (solid histogram). The expected distribution (arbitrary normalisation) for a signal of $M_{\tilde{\nu}} = 140$ GeV/c^2 and $M_{\chi} = 100$ GeV/c^2 (dashed histogram) is also indicated.

16
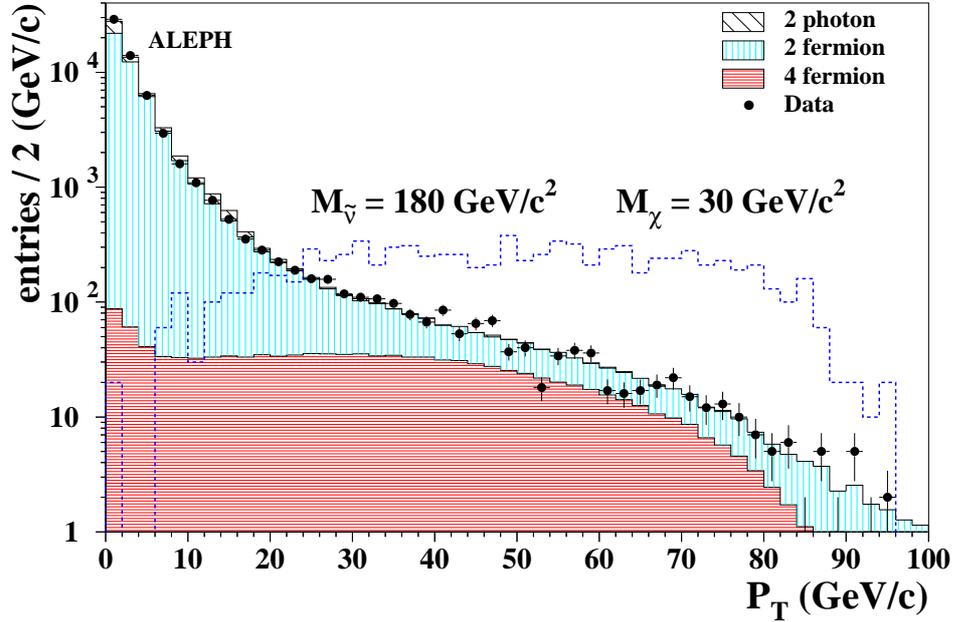
Figure 8: The distribution of the missing transverse momentum, at preselection level, for $\sqrt{s} = $ 189–209 GeV: data (dots with error bars), expected background (solid histogram). The expected distribution for a signal (arbitrary normalisation) with $M_{\tilde{\nu}} = 180 \, \text{GeV}/c^2$ and $M_{\chi} = 30 \, \text{GeV}/c^2$ is also indicated (dashed histogram).
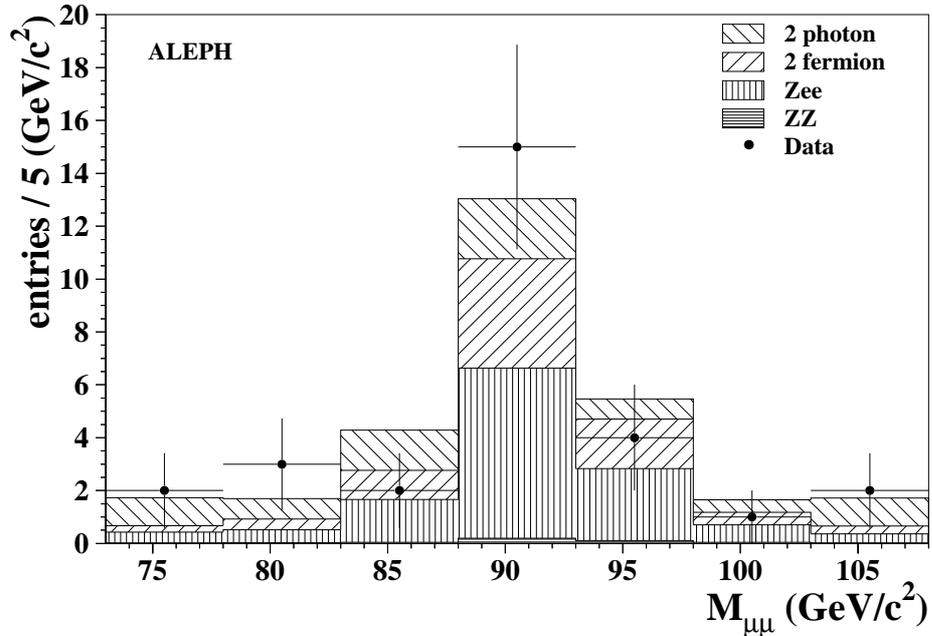

Figure 9: The invariant $\mu^+\mu^-$ mass distribution, obtained using a modified λ_{1j2} selection, for $\sqrt{s} = $ 189–209 GeV: data (dots with error bars), expected background (solid histogram).

17
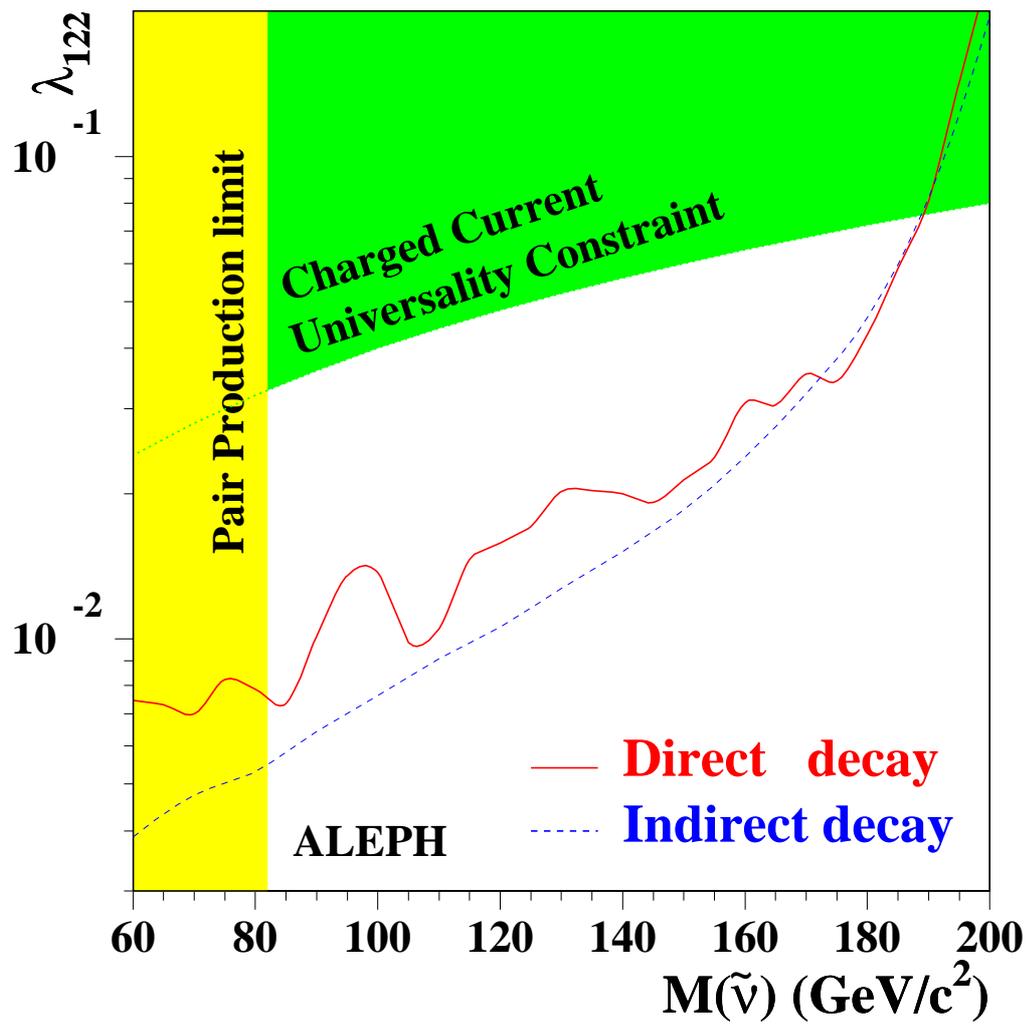
Figure 10: Observed 95% CL upper limits on the λ_{122} coupling for the direct and indirect decays. The exclusions from the low energy bounds and the pair production search are indicated.

Figure 11: Observed 95% CL upper limits on the λ_{123} coupling for the direct and indirect decays. The exclusions from the low energy bounds and the pair production search are indicated.
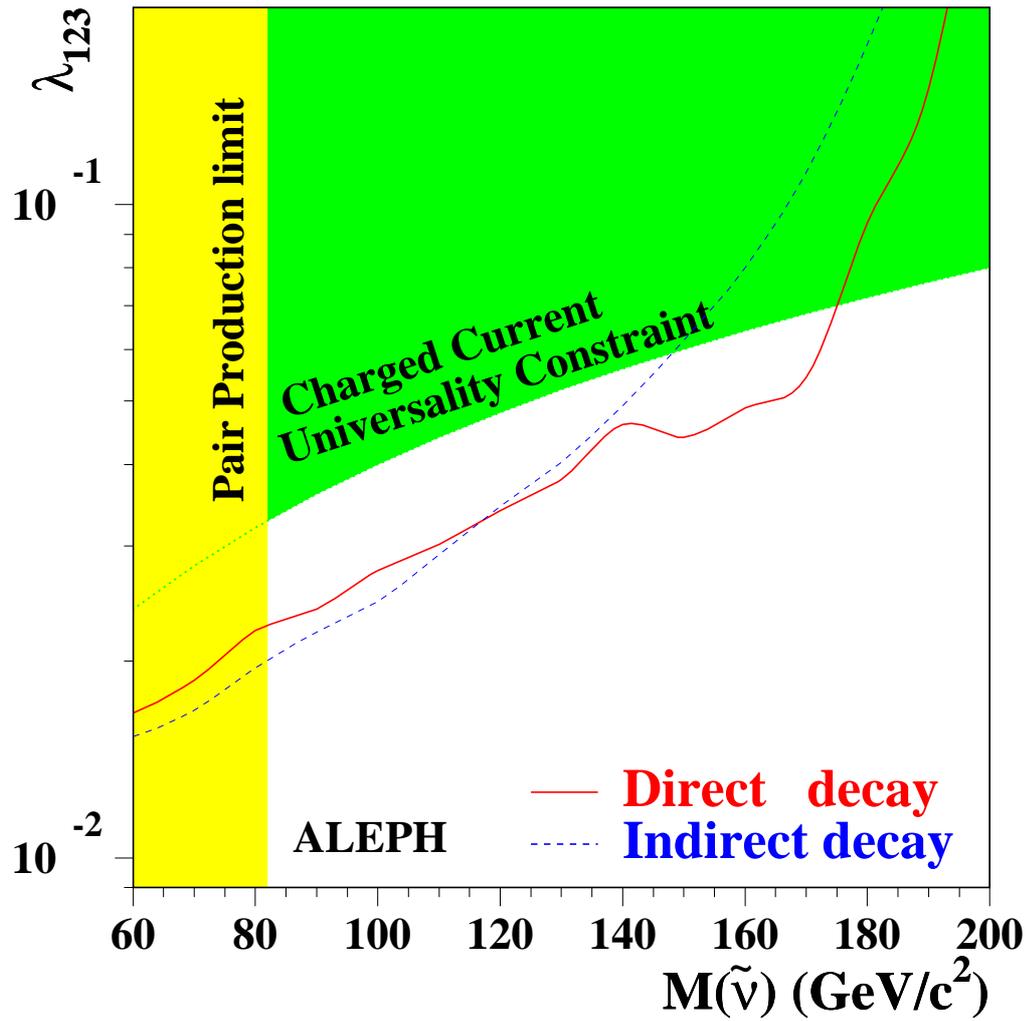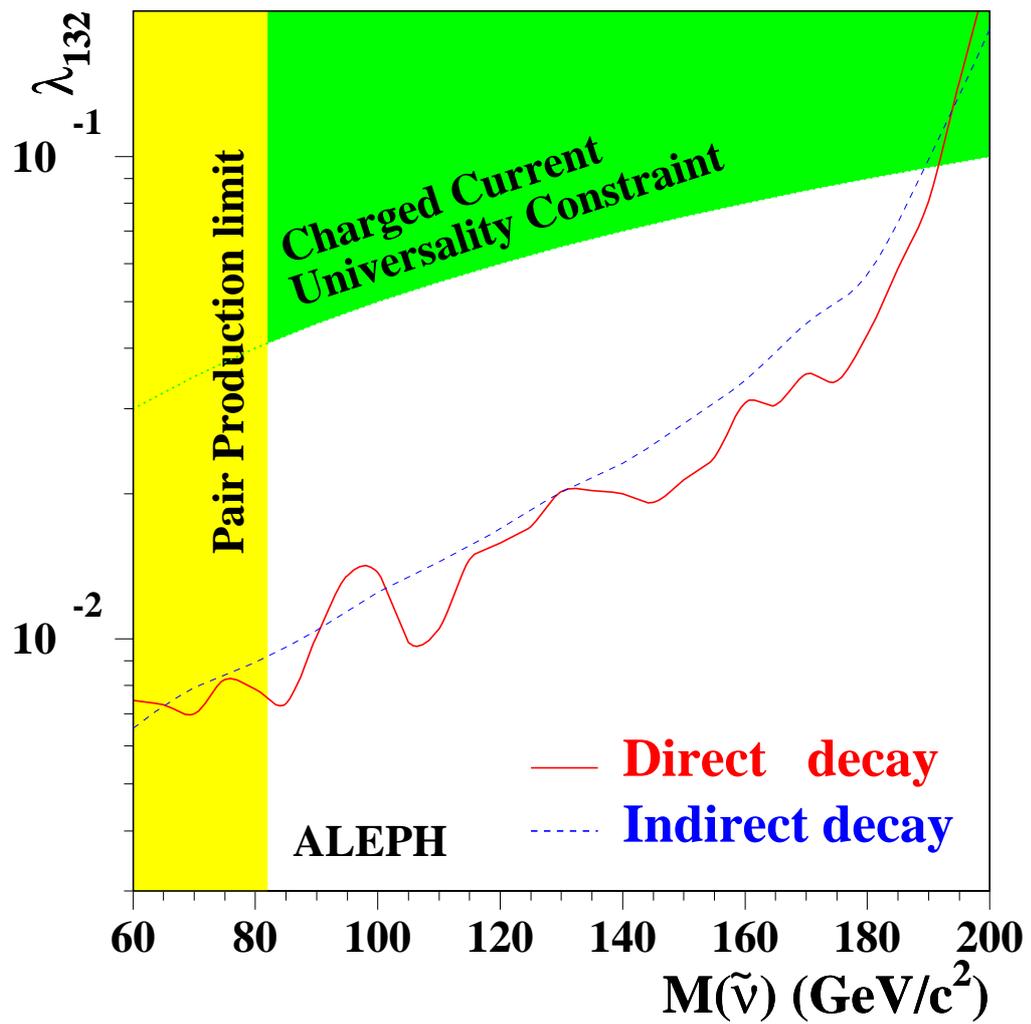
Figure 12: Observed 95% CL upper limits on the λ_{132} coupling for the direct and indirect decays. The exculsions from the low energy bounds and the pair production search are indicated.
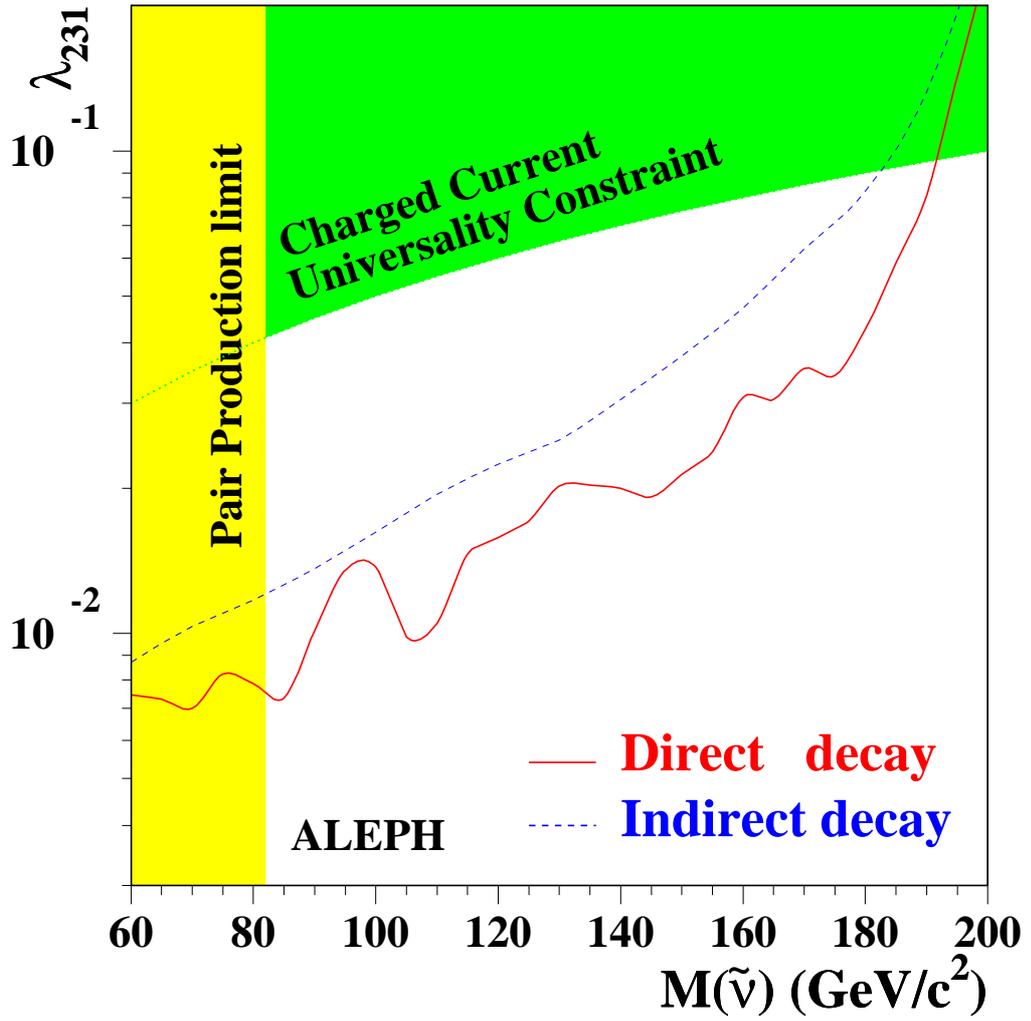
Figure 13: Observed 95% CL upper limits on the λ_{231} coupling for the direct (λ_{1j2} analysis used) and indirect decays. The exclusions from the low energy bounds and the pair production search are indicated.
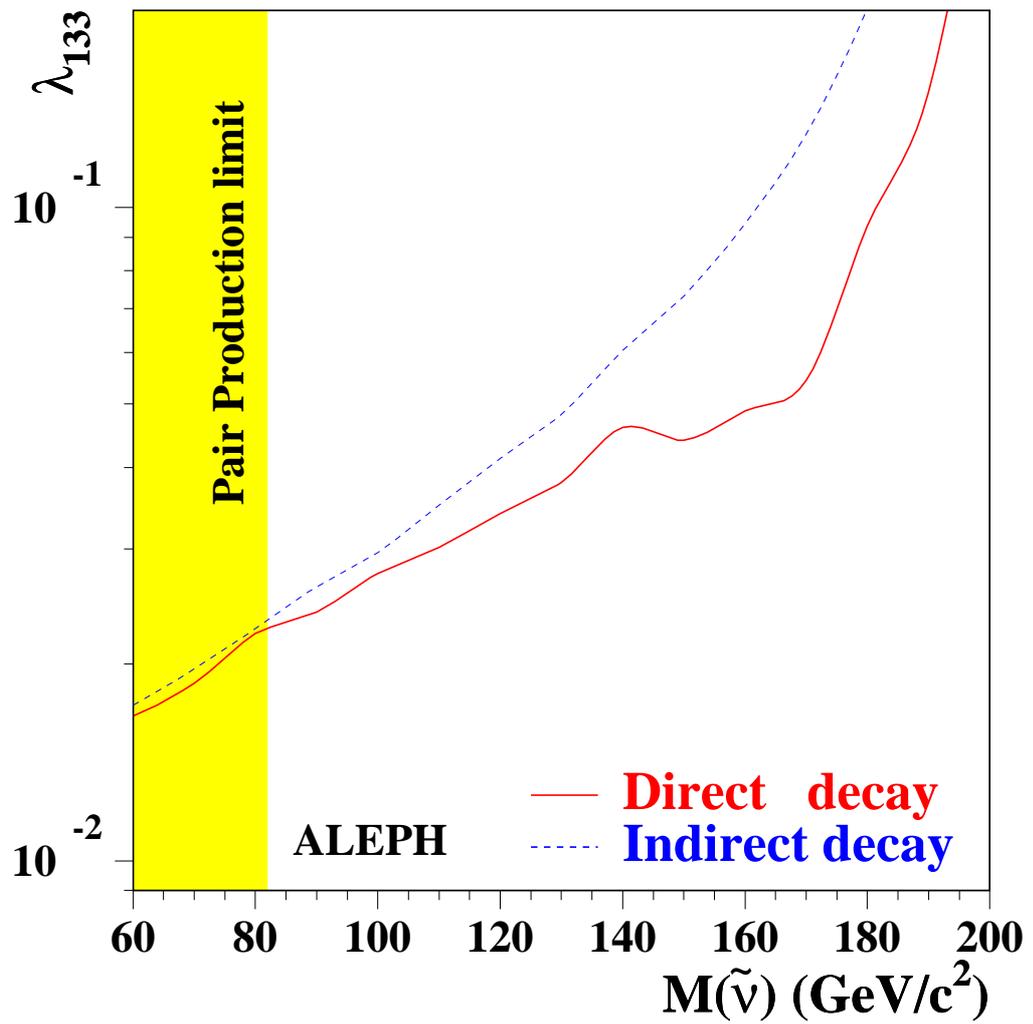
Figure 14:   Observed 95% CL upper limits on the λ_{133} coupling for the direct and indirect decays. The exclusion from the pair production search is indicated.